2013 IEEE/RSJ International Conference on
Intelligent Robots and Systems (IROS)
November 3-7, 2013. Tokyo, Japan

Design and Realisation of a Novel Robotic Manipulator for Retinal Surgery

A. Gijbels, N. Wouters, P. Stalmans, H. Van Brussel, D. Reynaerts, E. Vander Poorten

***Abstract*— Retinal Vein Occlusion (RVO) is a common retinal vascular disorder which may cause severe loss of vision. Retinal cannulation appears to be the most effective treatment, but given the small diameter of a retinal vein, it is too difficult and risky for a surgeon to perform this procedure manually. This work reports on the development of an innovative robotic manipulator to assist vitreoretinal surgeons during this procedure using a co-manipulation control strategy. The robotic manipulator features a new Remote-Center-of-Motion mechanism with four degrees of freedom. This mechanism is particularly interesting for applications in minimally invasive surgery where an instrument needs to be manoeuvred in a highly confined space around a fixed incision point. The developed manipulator is shown to be a great asset in improving the quality of retinal cannulations compared to the manual procedure. This is shown by cannulation experiments performed on a custom made eye model and an injectable retina model that effectively simulate real retinal cannulations.**

I. Introduction

A. Retinal Vein Occlusion (RVO)

RVO is an eye condition which affects an estimated 16.4 million adults worldwide [1]. The disease occurs when a clot is formed in a retinal vein. This causes the patient to slowly lose his/her sight. Fig. 1 shows a healthy retina on the left and a retina suffering from RVO on the right. Today, there is no proven effective treatment available for this disease [2]. A promising treatment is retinal vein cannulation. During this procedure the surgeon inserts a needle through the sclera and injects a small dose of t-PA, a clot-dissolving agent, directly into the blocked vein [3]. Fig. 2 conceptually demonstrates this procedure. Several research groups report successful cannulations in animal and human models. However, due to safety issues, the procedure is not performed clinically today. The needle needs to be inserted in a vein with a diameter smaller than 500 µm and kept there for several minutes for the fluid to be fully injected [4]. Unintended movements make it extremely difficult to insert and maintain the needle into the vein. They can cause serious damage to the retina during this procedure. Two relevant types of unintended movements can be distinguished. Firstly, the human suffers from physiological tremor. Hand vibrations with an rms amplitude of 182 µm during vitreoretinal procedures have been reported [5]. Secondly, the eye tends to rotate during the procedure due to the lateral forces applied by the instrument on the incision point. These rotations cause the retina to move which makes the surgeon to aim at a dynamic target.

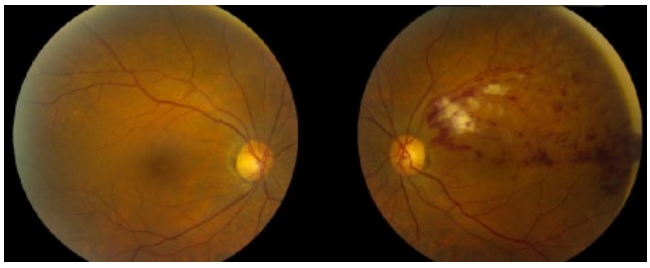

Fig. 1. Retinal Vein Occlusion: when a retinal vein gets blocked, the circulation of blood through the affected vein is reduced or stopped. The blockage causes the walls of the vein to leak blood and excess fluid into the retina. When the fluid collects in the macula (the area of the retina responsible for central vision), vision becomes blurry. Left: healthy retina. Right: retina with RVO.

Andy Gijbels, Niels Wouters, Hendrik Van Brussel, Dominiek Reynaerts and Emmanuel Vander Poorten are with the Department of Mechanical Engineering, University of Leuven, 3001 Heverlee, Belgium

Peter Stalmans is with the Department of Ophthalmology, University of Leuven, 3000 Leuven, Belgium

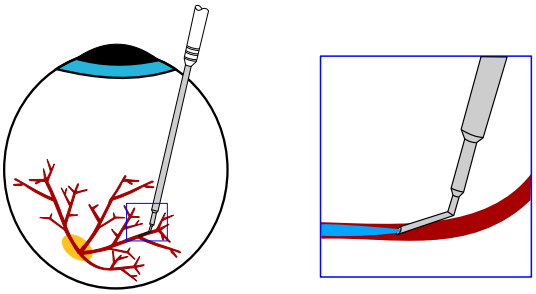

Fig. 2. Retinal Vein Cannulation: a hollow needle is inserted through the sclera and used to inject a clot-dissolving agent directly into the affected vein to remove the blockage causing RVO.

B. Robot-assisted retinal cannulations

Abovementioned problems can be overcome through the use of a robotic manipulator that assists the surgeon during the procedure. The instrument is attached to the manipulator at its end-effector. The surgeon co-operatively moves (co-manipulates) the instrument by gripping and manipulating the instrument. During this process the manipulator influences the instrument's motion in several ways. Firstly, physical and/or virtual damping in the manipulator can help to filter out the tremor. This damping also slows down the intended movements facilitating a slow and precise approach of the vein. Secondly, the system can maintain a stable position once the needle is inserted into the blocked vein allowing a steady and reliable t-Pa injection. Thirdly, the eye can be held stationary during the procedure by virtue of a Remote Center of Motion (RCM) incorporated in the manipulator. An RCM is a geometric point at a fixed location about which the

978-1-4673-6357-0/13/$31.00 ©2013 IEEE

instrument can pivot and translate through without a physical joint being present at this location [6]. When this RCM is made to coincide with the incision point in the sclera, the degrees of freedom (DOFs) of the instrument will be restricted to three rotations Θ, Φ and Ψ around the RCM and a translation R through the RCM as shown in Fig. 3. In this way, the eye and thus the retina are stabilized such that aiming at the blocked vein becomes easier. Using such a manipulator in a co-manipulation fashion poses some specific advantages compared to using it in a more common teleoperation fashion. When co-manipulating, the surgeon remains in close distance to the operating site. Therefore he/she keeps a good overview on the evolution of the surgical procedure and can respond quickly in case unforeseen situations arise. Furthermore, a robotic co-manipulator is potentially much cheaper and less complex to commercialise since only one device is needed.

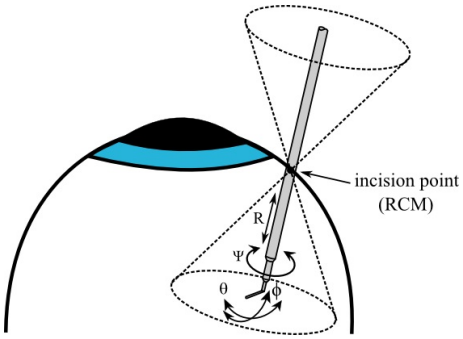

Fig. 3. Vitreoretinal surgeons only need 4 DOFs to manoeuvre the instrument in the eye: three rotations Θ, Φ and Ψ around the incision point and a translation R through the incision point. The remaining DOFs, which cause unintended eye rotations, can be blocked by aligning the RCM of the surgical manipulator with the incision point.

C. State of the art

A fair number of robotic systems developed for surgical assistance during vitreoretinal procedures have been reported in literature [7]–[11]. Apart from the difference in operation modus, i.e. co-manipulation or teleoperation, they further differ in the way the Remote Center of Motion is incorporated in the surgical manipulator. Generally speaking, one can distinguish two major ways of realising a RCM: through software (virtual RCM) or mechanically (real RCM). From a safety point of view, one can argue that a mechanical RCM is advantageous compared to a software-based RCM. Firstly, the required number of actuators to achieve the four DOFs is lower. This also positively affects the achievable accuracy since less errors are built up. Secondly, in case of power or sensor failure, the robot at least maintains the RCM and undesired movements of the instrument are still prohibited. Several mechanical RCM-based robotic devices for vitreoretinal surgery have been reported in literature. But most of them fail to keep the end-effector compact enough. This is problematic because of the very confined workspace typically for vitreoretinal surgery. The operating scene is populated by the patient, the surgeon and the microscope that the surgeon uses to navigate the instruments inside the patient's eye. Fig. 4 demonstrates the operating scene during a typical vitreoretinal procedure. To overcome these space limitations, a novel robotic manipulator based on an innovative RCM mechanism allowing a compact construction of the robotic end-effector is proposed and detailed here.

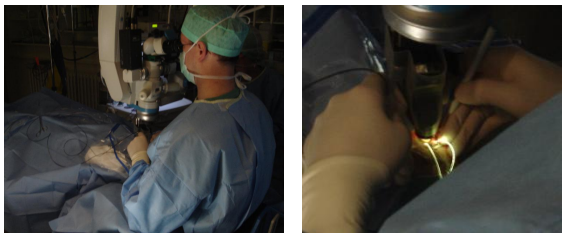

Fig. 4. Left: Surgical scene during a vitreoretinal procedure. Right: The surgeon needs to operate in a highly confined space due to the presence of the microscope and the spherical lens. The spherical lens is used to see the whole retina through the microscope without the necessity to move the eye.

II. Design of the Robotic Manipulator

A. Kinematic design requirements

Surgeons require an available area on the retina of 60° around the center of the eye to perform retinal cannulations. We chose to increase this range up to 90° to give the surgeon enough freedom to move during the procedure (see Fig. 5). To reach the retina with the needle, the surgeon always makes an incision point at 4 mm from the corneal limbus. This is because no vital tissue is present at this location. Given this information and taking into account the variety in eye dimensions among patients [12], the necessary ranges for the different DOFs can be calculated (see Table I).

In order to perform a cannulation without pushing the vein away or damaging it, the needle should be ideally inserted as close and parallel as possible to the longitudinal axis of the vein. This explains the use of a needle with a bended tip. Given the sizes of retinal veins and the fact the surgeon will always try to inject a bigger vein, a positioning accuracy of 10 µm at the tip of the needle should be sufficient. From this value the necessary positioning accuracy for the different DOFs can be calculated (see Table I). The accuracy for the Ψ-DOF is based on a 60 µm-diameter hooked needle tip inserted over 1 mm in an 80 µm-diameter vein.

TABLE I
Kinematic Design Requirements

	Tip	Θ	Φ	Ψ	R
Range		$+50°$	$\pm 28°$	$+360°$	30 mm
Accuracy	10 µm	$0,023°$	$0,023°$	$1°$	10 µm

B. Remote-Center-of-Motion mechanism

Despite the broad field of application of an RCM in minimally invasive surgery (MIS) and the advantages of having a mechanically constrained RCM, the number of instantations of RCM mechanisms remain fairly limited. Only a handful of substantially different mechanisms containing such a

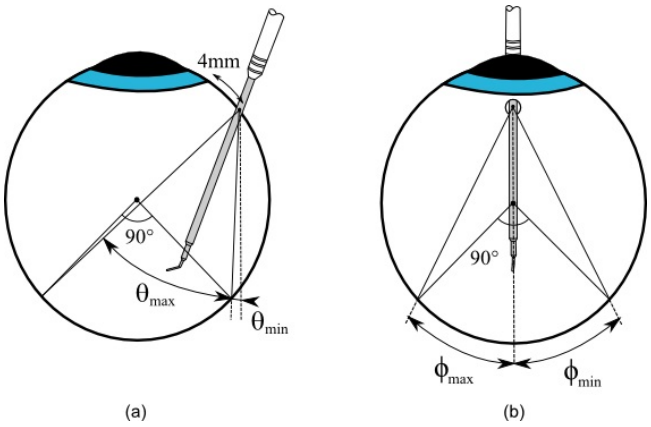

Fig. 5. Left: required work range in Θ. Right: required work range in Φ.

property have been reported. With very few exceptions all reported RCM mechanisms are either parallelogram-based, circular-prismatic-joint, synchronous-transmission-based or instantaneous RCM mechanisms [6]. The most common 2-DOF RCM mechanism is the double-parallelogram mechanism first introduced by Taylor et al. [13]. Fig. 6(a) shows this mechanism enabling the instrument to rotate in Θ and Φ around the RCM in point A. Note that stacking parallellograms BCFE and DFHG results in an imaginary parallellogram ACHG, explaining the RCM at A, like shown in Fig. 6(b). Because of the relatively large movement range and the simplicity of the structure, this mechanism has been widely adopted in robotic manipulators for MIS. The major concern when applying this mechanism for the intended application, consists in the way how the translational DOF is implemented in these robotic manipulators. In general, this is done by adding a linear drive mechanism at the end-effector conceptually depicted in Fig. 6(c). Note hereby the inclination of parallelogram BCFE which insures that the instrument's axis passes through the RCM in point A. Considering the tight space constraints associated with vitreoretinal procedures, like discussed earlier, such a voluminous end-effector is not desirable. One possible solution would exist in replacing this linear drive mechanism by two prismatic joints at the base of the mechanism in B and C as shown in Fig. 6(d). However, in this way links BE and CF can slide independently from each other, losing parallellogram BCFE and thus the imaginary parallelogram ACHG and the RCM. This is shown in Fig. 6(e). To prevent this, the extra linkage IJ was added to the mechanism in Fig. 6(d). Note that this mechanism can still lose the imaginary parallelogram ACHG and thus the RCM when parallelogram BCFE forms a rectangle as shown in Fig. 6(d). In this configuration, parallelogram BCFE can transform into a trapezium when BE and CF start sliding in opposite directions like shown in Fig. 6(f). In order to guarantee a fixed RMC, a method should be found to keep the imaginary parallelogram ACHG intact at all times. This can be done by using the mechanism shown in Fig. 6(g). The mechanism contains three parallelograms: DEHG, CBJI and IJFH. Because linkages IJ and BC and linkages HF and IJ respectively remain parallel at all times, linkages GH and AC of the imaginary parallelogram ACHG will remain parallel as well. Parallelogram DEHF keeps the linkages CH and AG parallel. Since linkage CH can translate through the prismatic joint in C, linkage AC, and thus the instrument, are able to translate through the RCM in A. The Ψ-DOF is added locally at the end-effector since this can be done in a compact way. Fig. 6(h) shows a combination of a translation and a rotation of the instrument in the *R*Θ-plane demonstrating the RCM.

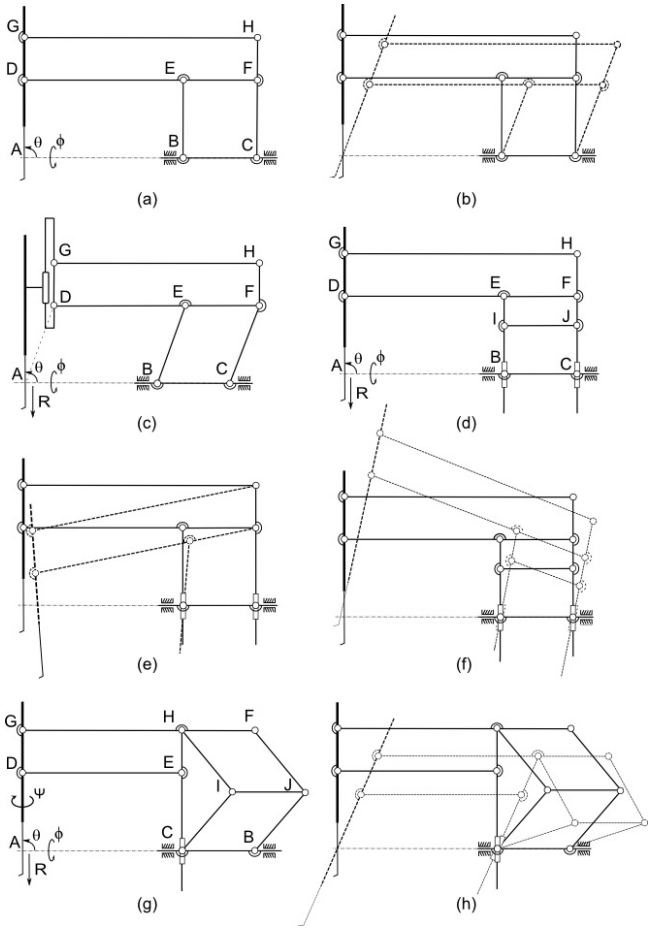

Fig. 6. The double-parallellogram RCM mechanism of Taylor et al. [13] has been widely applied in the design of surgical manipulators (Fig. 6(a)-(c)). Trivial attempts to keep the end-effector compact by implementing the linear DOF at the base of the mechanism, fail to maintain the RCM (Fig. 6(d)-(f)). A new tripple-parallellogram RCM mechanism enabling the linear DOF at the base of the mechanism, is proposed (Fig. 6(g)-(h)).

C. Kinematics and dimensioning of the RCM mechanism

In the below, the 4-DOF RCM mechanism of Fig. 6(g). is further dimensioned for the intended application. The final mechanism is shown in Fig. 7.

1) Actuation of the different degrees of freedom:

Multiple possibilities exist to drive the *R*- and Θ-DOF. Calculations show that when rotary actuators are used, actuating the angles of linkages l_5 and l_8 results in the most uniform and isotropic manipulability. To limit the inertia of the system, it is desirable to locate the actuators at the base of the mechanism. Since this is not directly possible for the actuation of linkage l_8, the extra linkages l_{10} and l_{11} were

added. Since linkage l_{10} always remains parallel to linkage l_8, linkage l_{10} can be actuated instead of linkage l_8 without changing the manipulability of the mechanism. The Φ-DOF is directly driven by a rotary actuator. Since precision is of much lower importance for the Ψ-DOF (see Table I), this DOF is left unactuated. Given this actuation sheme the Jacobian $\mathbf{J}$, which maps the joint velocities $\dot{q}_1$, $\dot{q}_2$ and $\dot{q}_3$ to the end-effector translational and rotational velocities $\dot{R}$, $\dot{\theta}$ and $\dot{\psi}$, can be formulated as

$$\begin{bmatrix} \dot{R} \\ \dot{\Theta} \\ \dot{\Phi} \end{bmatrix} = \mathbf{J}(\mathbf{q}) \begin{bmatrix} \dot{q}_1 \\ \dot{q}_2 \\ \dot{q}_3 \end{bmatrix}, \quad \text{with} \quad \mathbf{J}(\mathbf{q}) = \begin{bmatrix} \frac{A}{\sqrt{E}} & \frac{B}{\sqrt{E}} & 0 \\ \frac{C}{E} & \frac{D}{E} & 0 \\ 0 & 0 & 1 \end{bmatrix} \tag{1}$$

and

$$\begin{aligned} A &= (l_{4_2} - l_{0_1}) l_5 \sin(q_1) - l_5 l_8 \sin(q_1 - q_2), \\ B &= (l_{4_2} - l_{0_1}) l_8 \sin(q_2) + l_5 l_8 \sin(q_1 - q_2), \\ C &= (l_{0_1} - l_{4_2}) l_5 \cos(q_1) + l_5 l_8 \cos(q_1 - q_2) + l_5^2, \\ D &= (l_{0_1} - l_{4_2}) l_8 \cos(q_2) + l_5 l_8 \cos(q_1 - q_2) + l_8^2, \\ E &= [l_5 \cos(q_1) + l_8 \cos(q_2) + l_{0_1} - l_{4_2}]^2 + \ldots \\ &\quad \ldots + [l_5 \sin(q_1) + l_8 \sin(q_2)]^2. \end{aligned}$$

Solving the equation $det(\mathbf{J}(\mathbf{q})) = 0$, shows that the mechanism possesses singularities for $q_1 = q_2$ and for $q_1 = -q_2$. These singularities correpond to the configurations where parallelograms GHJI and IJLK are aligned with one another.

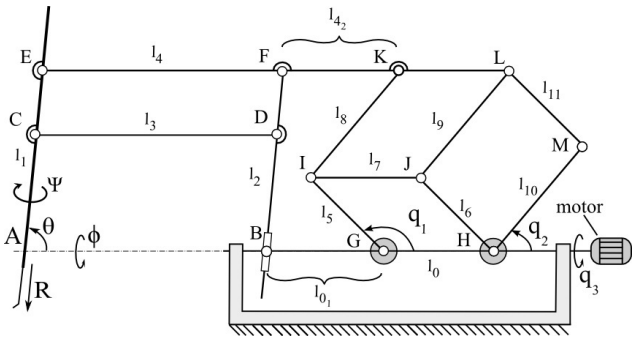

Fig. 7. The final 4-DOF RCM mechanism.

2) Designing the workspace:

To fit the workspace of the mechanism to the kinematic requirements listed in Table I, two measures were taken. Linkages l_8, l_9 and l_{10} were made longer compared to linkages l_5, l_6 and l_{11}. This action gives an inclination to the neutral configuration of the mechanism compared to the mechanism shown in Fig. 6(g). To further increase this effect, while limiting the size of the mechanism, linkage l_{0_1} is made longer than linkage l_{4_2}. The workspace of the needle tip in the $R\Theta$-plane is limited by collisions which can take place between the individual linkages. The following conditions describe these limitations:

$$\begin{aligned} &q_1 \approx [65^\circ, 137^\circ], && q_2 \approx [25^\circ, 119^\circ], \\ &q_3 = [-45^\circ, 45^\circ], && q_1 \geq q_2 + 18^\circ, \\ &\Theta \geq 40^\circ. \end{aligned} \tag{2}$$

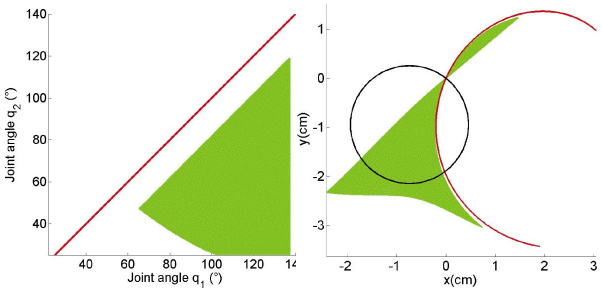

(a) (b)

Fig. 8. The joint (left) and Cartesian (right) workspace (green) in the $R\Theta$-plane. The red line corresponds to the singular configurations. The black circle represents a cross section of the eye.

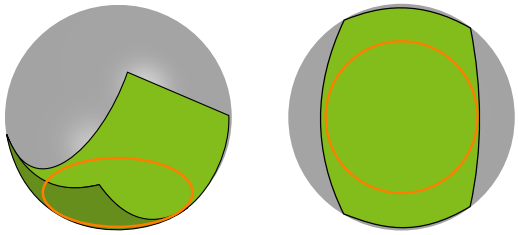

Fig. 9. The workspace of the surgical manipulator (green) successfully covers the required workspace (orange). Left: Retinal workspace in 3D. Right: top view on the retinal workspace.

The resulting joint workspace for the $R\Theta$-mechanism is shown in Fig. 8(a). The red line indicates the singularities when $q_1 = q_2$. These singularities form no problem as they lie outside the manipulator workspace. The Cartesian workspace (Fig. 8(b)) can be calculated by using the forward kinematic equations:

$$\begin{aligned} R &= -l_1 + \sqrt{[l_5 \cos(q_1) + l_8 \cos(q_2) + l_{0_1} - l_{4_2}]^2 + \ldots} \\ &\quad \overline{\ldots + [l_5 \sin(q_1) + l_8 \sin(q_2)]^2}, \\ \Theta &= \arctan\left(\frac{l_5 \sin(q_1) + l_8 \sin(q_2)}{l_5 \cos(q_1) + l_8 \cos(q_2) + l_{0_1} - l_{4_2}} \right), \\ \Phi &= q_3. \end{aligned} \tag{3}$$

Finally, the workspace on the retina is calculated and compared to the kinematic requirements of Table I. The results are shown in Fig. 9 where the green area represents the manipulator workspace and the orange line the required workspace. This figure clearly shows that the design requirements are met.

D. Design details of the manipulator

Fig. 10 shows the final design of the robotic manipulator. The symmetrical design places the center of mass in a vertical plane through the central axis, which prevents unwanted tilting. The linkages are H-shaped and fit into each other to enable a collision-free movement. The $R\Theta$-mechanism is mounted in a base which carries the motors and encoders for these DOFs. The Ψ-DOF is implemented in the instrument holder. The Φ-DOF is implemented by the rotation of the mechanism around the central axis of the support structure. The manipulator is designed to be backdrivable by using direct drives for the R- and Θ-DOF

and a capstan cable drive mechanism for the Φ-DOF. In this way friction and play are limited to a minimum. The backdrivability of the mechanism makes it possible for the surgeon to co-manipulate the manipulator without requiring a force sensor upon the mechanism. All drives use Maxon DC-motors. Most of the required torque to drive the mechanism results from overcoming gravity. To compensate for this effect the manipulator was made out of aluminium 7075. This is a light but very strong alloy. The weight of the bar mechanism is limited to 1.47 kg. The effects of gravity are further decreased by using two counterweights limiting the maximum torque to 0.062 Nm. To achieve the desired positioning accuracy at the tip of the needle, GPI 9211S encoders with a resolution of 144000 counts per revolution are used for the direct drives and a GPI R120 encoder with 65536 counts per revolution for the capstan drive. Fig. 11 shows the realisation of the robotic manipulator. The overall dimensions of the manipulator are $27 \times 37 \times 20$ cm.

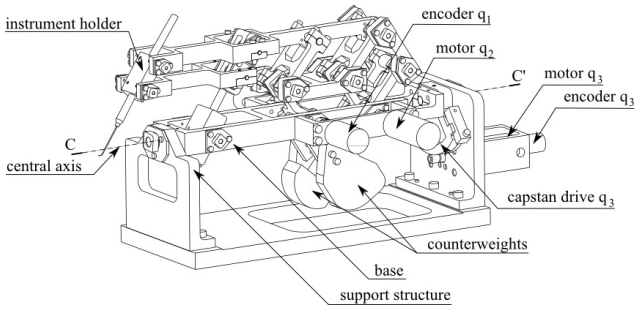

Fig. 10. Final design of the robotic manipulator.

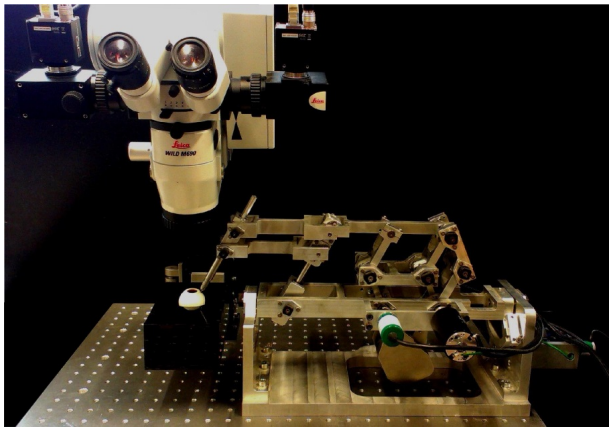

Fig. 11. The realised robotic manipulator.

E. Design of a co-manipulation controller

The different motions occurring during a retinal cannulation can be grossly divided into three types of manoeuvres (see Fig. 12). Firstly, the surgeon needs to put the needle through the incision point and cross the eye diameter before reaching the retina. This action is characterized by a relatively long distance which can be covered relatively quick. Secondly, he/she needs to carefully insert the needle into the blocked vein. This action requires accurate positioning and thus slow movements. Thirdly, once in the vein, the surgeon needs to keep the needle as steady as possible while the fluid is being injected. Ideally, no movements take place during this action. Afterwards the surgeon gently retracts the needle from the vein and the eye. The latter manoeuvres fundamentally don't differ from the aiming and approaching manoeuvres respectively. For each of these manoeuvres an ideal instrument behavior is defined. During the approaching phase the surgeon wants to freely move the instrument, so no virtual damping is required (damping $c = 0$ Ns/m). During the aiming phase virtual damping can be added to damp out hand vibrations and to slow down the intended movements for more precise positioning ($c = c_{max}$). During the injection phase, the needle tip must be kept as still as possible inside the vein. This can be done by attaching a virtual spring-damper between the tip of the needle and the vein center (spring stiffness $k = k_{max}$, $c = c_{max}$). To implement this instrument behavior, the following control law is implemented:

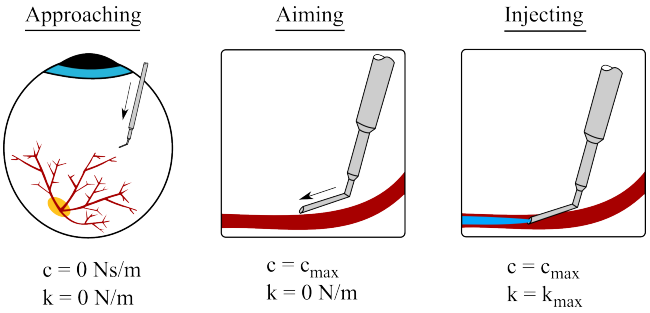

Fig. 12. The cannulation procedure can be divided into three actions: approaching, aiming and injecting. Each action requires a specific behaviour (damping c and stiffness k) from the surgical manipulator to be successful.

$$\tau(\mathbf{q}, \dot{\mathbf{q}}, p_{pedal}) = \mathbf{J}^{\mathbf{T}}(\mathbf{q})\mathbf{F}(\mathbf{q}, p_{pedal}) + \tau_{\mathbf{G}}(\mathbf{q}) \quad (4)$$
$$\mathbf{F}(\mathbf{q}, \dot{\mathbf{q}}, p_{pedal}) = \mathbf{c}(p_{pedal})\mathbf{J}(\mathbf{q})\dot{\mathbf{q}} + \mathbf{k}(p_{pedal})FKE(\mathbf{q} - \mathbf{q_{hold}})$$

where τ is the vector with motor torques, p_{pedal} is the position of a foot pedal, $\mathbf{J}^{\mathbf{T}}$ is the transpose of the Jacobian, $\mathbf{F}$ is a vector with the forces applied to the instrument handle by the manipulator in each DOF, $\tau_{\mathbf{G}}(\mathbf{q})$ is a vector with the torques for the gravitation compensation of the manipulator, FKE are the forward kinematic equations as in (3), $\mathbf{c}$ and $\mathbf{k}$ are vectors with the virtual damping factors and stiffnesses respectively in each DOF, $\mathbf{q}$ and $\dot{\mathbf{q}}$ are vectors representing the joint positions and velocities of the manipulator respectively and $\mathbf{q_{hold}}$ is the vector with the joint positions when the foot pedal is being released.

With the footpedal the surgeon himself/herself can control the overall behavior of the manipulator. When the pedal is fully pressed, no virtual damping or stiffness is applied to the instrument. The more the surgeon releases the foot pedal, the more virtual damping is applied to the instrument. When the foot pedal is fully released the instrument is locked into its current position using the maximum virtual damping and stiffness. To compensate for the remaining gravitational forces of the manipulator on the instrument, a gravitation compensation was implemented in the controller.

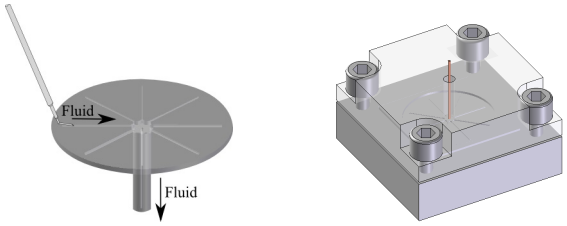

(a) (b)

Fig. 13. A PDMS retina mock-up (left) was made by pouring a mixture of PDMS elastomer and a curring agent into a hot mold (right). The top of the retina is closed by a spin coating procedure. The retina consists of 80 μm-500 μm beam-shaped channels which act as veins.

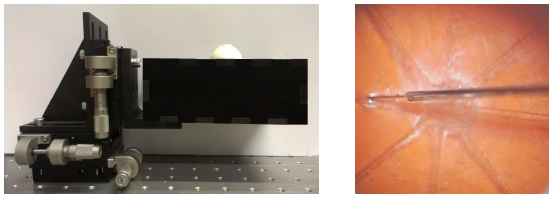

(a) (b)

Fig. 14. An artificial eye (left) with a polymer retina (right) is connected with a gimbal mechanism inside the black box to simulate the human eye and its movements. The system is attached to a XYZ stage to align the incision point in the eye with the RCM of the surgical manipulator.

Notice the user forces are only indirectly used in this control sheme. Since the manipulator is back-drivable the control can be done using solely the joint positions and velocities and the foot pedal position.

III. Experimental validation

To validate the robotic manipulator, a mock-up of the eye and the retina were built to simulate retinal cannulations in an efficient and repeatable way. Fig. 13(a) displays the concept behind this retinal cannulation simulation. When fluid is succesfully injected into a channel of the retina model, it flows to the center of the retina and exits the eye through a central tube. Retina samples are made out of a heat-curable flexible polymer using the mold shown in Fig. 13(b) and a spincoating machine to seal the top of the retina model. The length of the sides of the embedded beam-shaped channels in the retina model range from 80 μm to 500 μm. The retina model is placed into a polymer eye. To enable the rotation of the eye in Φ and Θ, the eye is placed into a custom made gimbal mechanism. To align the incision point with the manipulator's RCM, the mockup is placed on an XYZ-platform. Fig. 14(a) and 14(b) show the total test setup and the polymer retina respectively. Video recordings, in attachment to this paper, where a 200 μm-channel was cannulated using a 80 μm needle, show that the manipulator indeed stabilizes the eye, reduces tremor and keeps the needle steady once inside the channel.

IV. Conclusion and Future work

We successfully designed and built a novel robotic manipulator to assist vitreoretinal surgeons during retinal cannulations. The system relies on a novel RCM mechanism which implements the translational degree of freedom of the instrument at the base of the mechanism. In this way the end-effector is held very compact, which is particularly interesting for applications where the end-effector needs to manoeuvre in a highly confined space. The RCM mechanism was further optimized for the specific application of retinal vein cannulation. Two direct drive systems and a capstan drive mechanism are used to implement an appropriate control strategy for this procedure and to keep the manipulator backdrivable. To test the device, we simulated a retinal cannulation using a custom made eye and retina model. During an initial experiment, the benefits of using the robotic manipulator compared to the manual procedure already became clear. More experiments will be done in the near future to quantify the differences between a manual and a robot-assisted procedure. To align the RCM of surgical manipulator with the incision point, the manipulator will be mounted on a custom-made XYZ-platform.

V. Acknowledgments

This work was supported by an FP7-People Marie Curie Reintegration Grant, PIRG03-2008-231045 and by a PhD grant from the Institute for the Promotion of Innovation through Science and Technology in Flanders (I.W.T.-Vlaanderen), 101445

References

[1] R. Sophie, "The prevalence of retinal vein occlusion: Pooled data from population studies from the united states, europe, asia, and australia," *Ophthalmology*, vol. 117, pp. 313– 319, 2010.

[2] B. Nilufer and B. Cosar, "Surgical treatment of central retinal vein occlusion," *Acta Ophthalmologica*, vol. 86, pp. 245–252, 2008.

[3] L. A. Bynoe, R. K. Hutchins, H. S. Lazarus, and M. A. Friedberg, "Retinal endovascular surgery for central retinal vein occlusion: Initial experience of four surgeons," *Retina*, vol. 25, pp. 625–32, 2005.

[4] M. R. Glucksberg, R. Dunn, and C. P. Giebs, "In vivo micropuncture of retinal vessels," *Graefe's Archive for Clinical and Experimental Ophthalmology,*, vol. 231, pp. 405–407, 1993.

[5] C. N. Riviere and P. S. Jensed, "A study of instrument motion in retinal microsurgery," *Proc. of the 22nd Annual EMBS Int. Conf.*, 2000.

[6] G. Zong, X. Pei, J. Yu, and S. Bi, "Classification and type synthesis of 1-dof remote center of motion mechanisms," *Mechanism and Machine Theory*, vol. 43, pp. 1585 – 1595, 2008.

[7] K. Grace, J. Colgate, M. Glucksberg, and J. Chun, "A six degree of freedom micromanipulator for ophthalmic surgery," *IEEE Int. Conf. on Robotics and Automation*, vol. 1, pp. 630–635, 1993.

[8] M. Wapler, V. Urban, T. Weisener, J. Stallkamp, M. Durr, and A. Hiller, "A stewart platform for precision surgery," *Transactions of the Institute of Measurement & Control*, vol. 25-4, p. 329, 2003.

[9] Y. Ida, N. Sugita, T. Ueta, Y. Tamaki, K. Tanimoto, and M. Mitsuishi, "Microsurgical robotic system for vitreoretinal surgery," *Int. Conf. of Computer Assisted Radiology and Surgery*, pp. 27–34, 2012.

[10] A. Uneri, M. Balicki, J. Handa, P. Gehlbach, R. Taylor, and I. Iordachita, "New steady-hand eye robot with microforce sensing for vitreoretinal surgery research," *Int. Conf. on Biomedical Robotics and Biomechatronics*, pp. 814–819, 2010.

[11] Meenink, H.C.M., Rosielle, P.C.J.N., Steinbuch, and M. Smet, "Instrument manipulator for a master-slave robot for vitreo-retinal ophthalmic surgery," *Proc. of the 21st Int. Conf. on Medical Innovation and Technology 2009, Romania,*, p. 53.

[12] M. Charles and N. Brown, "Dimensions of the human eye relevant to radiation protection," *Physics in Medicine and Biology*, vol. 20(2), pp. 202–218, 1975.

[13] R. H. Taylor, J. Funda, D. D. Grossman, J. P. Karidis, and D. A. LaRose, "Us patent 5397323: Remote center-of-motion robot for surgery," 1995.